

Interaction between a pair of particles settling in a stratified fluid

A. Doostmohammadi and A. M. Ardekani*

Aerospace and Mechanical Engineering, University of Notre Dame, Notre Dame, Indiana 46556, USA

(Received 16 January 2013; revised manuscript received 12 June 2013; published 30 August 2013)

The anisotropic structure of fluidized suspensions is governed by their microstructures which are in turn determined by the dynamics of particle pair interactions. Here, we present a numerical simulation of particle interaction in linearly stratified fluids. It is shown that unlike homogeneous fluids, stratification results in the attraction of particles settling abreast. The attraction between the particles is characterized by the combined effects of buoyancy, inertia, and diffusion. The interaction of the particles settling in tandem can be fundamentally altered due to the presence of the background density gradients and the drafting-kissing-tumbling behavior in a homogeneous fluid can be replaced by drafting-kissing-separation or drafting-separation phenomenon depending on the strength of the stratification. In the case of weak stratification, drafting-kissing-tumbling occurs, however, a prolonged kissing time is observed and the rate of change of the orientation of particles is reduced. It is shown that the formation of the buoyancy-induced vortical structures and the generation of stratified jets behind the particles are the fundamental mechanisms in governing the dynamics of the particle pair interaction in stratified fluids.

DOI: [10.1103/PhysRevE.88.023029](https://doi.org/10.1103/PhysRevE.88.023029)

PACS number(s): 47.55.Hd, 92.20.Vn, 47.55.Kf, 91.50.Jc

I. INTRODUCTION

The sedimentation of suspended particles plays a major role in the ecology and pollution of environmental systems such as oceans and atmosphere [1,2]. Many of these systems are characterized by density gradients due to temperature and/or salinity differences between fluid layers. Understanding the stratification impact on the sedimentation is essential in a number of environmental processes and geophysical contexts such as urban pollution [3], sedimentary fluxes in the ocean [4], and carbon sequestration [5]. The vertical migration of marine snow particles made of organic matters such as dead parts of animals, plants, sand, and inorganic dust, is one of the main processes in transferring carbon between the ocean layers. Allredge and Gotschalk [6] showed that the accumulation of marine snow particles peak up to ten folds at regions of large density gradients in the ocean. In addition, phytoplankton consume carbon dioxide for their photosynthesis and after they die, they sediment to the deep ocean, leading to the transfer of approximately 10 gigatonnes of CO₂ every year from the atmosphere to the ocean [7]. Doostmohammadi *et al.* [8] recently demonstrated that the life of even small organisms can be markedly affected by the density stratification. Despite these widespread implications of sedimentation in stratified fluids the vertical motion of interacting particles in stratified fluids has received much less attention compared to the settling of an isolated particle, and the underlying hydrodynamics is yet to be explored.

The considerable drag increase during the vertical motion of a single particle in the presence of vertical density gradients has been studied both experimentally and numerically [9–14]. The settling velocity of a particle is suppressed in a stratified fluid and the combined effects of inertia, viscosity, buoyancy, and diffusion can affect the settling dynamics. For a particle of diameter d_p , moving with the velocity W_p , in a fluid with kinematic viscosity ν , the ratio of inertial forces to the viscous forces is defined by the Reynolds number, $Re_p = W_p d_p / \nu$. The relative importance of inertia and buoyancy effects is

described by the Froude number, $Fr_p = W_p / (Nd_p)$, where $N = (\gamma g / \rho_0)^{1/2}$ is the Brunt-Väisälä frequency corresponding to the natural frequency of oscillation of a vertically displaced parcel in a stably stratified environment, g is the acceleration due to gravity, γ is the background density gradient, and ρ_0 is a reference density. The diffusion impact is characterized by the Prandtl number, $Pr = \nu / \kappa$, the ratio of the momentum diffusivity to the diffusivity of the stratifying agent.

In the low Reynolds number regime, Yick *et al.* [14] demonstrated a drag enhancement of a falling sphere in a linearly stratified fluid due to the viscous entrainment of the fluid from upper density layers and the formation of a shell of lighter fluid behind the particle. In a recent theoretical study, Ardekani and Stocker [15] employed a point force singularity to model the far field behavior of settling particles in the Stokes regime and showed a substantial change in the flow field due to the presence of density gradients. The numerical study of Torres *et al.* [12] on the flow past a sphere in a linearly stratified fluid showed that at moderate Reynolds numbers the drag increase is due to the collapse of the rear vortices and the generation of a jet behind the particle. The experiments of Hanazaki *et al.* [16] for a wide range of Reynolds and Froude numbers ($30 < Re_p < 4000, 0.2 < Fr_p < 70$) illustrated that the generation of the jet can be markedly affected by the stratification and results in the formation of distinct columnar structures (jets) behind the particle. Bush *et al.* [17] compared the motion of particle clouds in homogeneous and stratified ambients and recognized distinct modes of particle deposition in a stratified fluid including localized, dispersed, and ring-shaped deposits. The missing part in all of these studies is the effect of stratification on the interaction of settling particles.

The sedimentation of a particle pair in a homogeneous fluid has been extensively studied. Fortes *et al.* [18] described the in-line settling of two identical particles as a three-stage process, “drafting, kissing, and tumbling (DKT).” For the system of two particles falling in tandem, the first stage corresponds to the acceleration of the trailing particle due to the wake behind the leading particle. In the second stage, two particles collide and form an unstable elongated body which tumbles due to inertial effects. They showed that this repeating

*aardekan@nd.edu

three-stage process can explain the nonlinear behavior of particle layers in homogeneous fluidized beds. In a viscoelastic fluid, however, the experiments of Riddle *et al.* [19] showed the existence of a critical distance above which the particles separate and never collide. Joseph *et al.* [20] demonstrated that particle pair interaction in a Newtonian fluid is dramatically different from a viscoelastic fluid where drafting, kissing, and chaining is the primary mechanism governing the interaction process. The results of [21] showed that kissing in a viscoelastic fluid is of a different nature and is because of the reversal of the pressure due to the presence of normal stresses in viscoelastic fluids. Also unlike the Newtonian fluid, the long bodies formed by kissing spheres can be stable in a viscoelastic fluid and the chaining of particles can occur. In addition, they showed that while side-by-side particles disperse in a homogeneous fluid, they can aggregate in a viscoelastic fluid.

Here, we provide a fully resolved three-dimensional direct numerical simulation of a pair of interacting spherical particles settling in a linearly stratified Newtonian fluid. We present distinct dynamical behaviors due to the presence of the background density gradients and demonstrate the decisive role of the stratification in characterizing the interaction between particles. We show that stratification markedly suppresses the dispersion of the particles settling abreast and even leads to aggregation of the particles. We demonstrate that a pair of particles settling in tandem undergo drafting-kissing-separation instead of drafting-kissing-tumbling when the Froude number is less than a critical value. Moreover, we present a stratification regime for which kissing does not occur and the initial drafting is followed by the particle separation. We show that the combined effects of buoyancy and inertia play a pivotal role in controlling the distance between particles and their interaction. For a weak stratification, we document a prolonged kissing time and slower change in the orientation of particles in stratified fluids. The results of this study can be applied to a wide range of sedimentation problems in natural and industrial environments and provide the basic step in characterizing microstructures of particulate flows of stratified fluids.

II. FORMULATION OF THE PROBLEM

The interaction of two rigid spherical particles in the presence of the background density gradient is simulated in a channel with a square cross section. The walls of the channel are set sufficiently far from the particles to minimize the wall effects on the particle motion. The particles are initially at rest and fall due to the action of gravity. A background density gradient is imposed by prescribing a linear temperature profile in the domain as the initial condition. The temperature is then linked to the fluid density by $\rho_f = \rho_0(1 - \beta T)$, where ρ_0 is the reference fluid density, background density at the initial location of the trailing particle, β the coefficient of thermal expansion, and T is the temperature. The particles are set to be adiabatic by imposing zero normal gradient condition $\partial T / \partial \mathbf{n} = 0$ on their surfaces, where \mathbf{n} denotes the unit vector normal to the surface of the particle.

The coupling between fluid flow and solid body motion is obtained through a two-step procedure. In the first step, the entire domain is considered as a fluid and fluid flow equations

are solved in the entire domain

$$\nabla \cdot \mathbf{u} = 0, \quad (1)$$

$$\tilde{\rho} \frac{D\mathbf{u}}{Dt} = -\nabla p + \mu \nabla^2 \mathbf{u} + (\rho - \tilde{\rho}) \mathbf{g} + \mathbf{f}, \quad (2)$$

$$\frac{\partial T}{\partial t} + \mathbf{u} \cdot \nabla T = D \nabla^2 T. \quad (3)$$

Following the Boussinesq approximation, the effects of density variations are only included as a source term in the momentum equation. In the above equations, \mathbf{u} is the velocity, p the pressure, \mathbf{g} the acceleration due to gravity, D the diffusivity of the stratifying agent, $\tilde{\rho} = \rho_p \phi + \rho_0(1 - \phi)$, and ϕ is the indicator function representing the volume fraction of grid cells occupied by solid particles. The term $\rho \mathbf{g}$ at the right-hand side of Eq. (2) accounts for the buoyancy effects where ρ is the total density defined as $\rho_p \phi + \rho_f(1 - \phi)$. The volume average of the total density over the computational domain, i.e., $\bar{\rho} = \int \rho dV / V$, is subtracted from the total density to avoid a uniform acceleration of the domain. It should be noted that the same governing equations apply to salt stratified fluids. In that case, T , D , and β represent the salt concentration, diffusivity, and salinity contraction coefficient, respectively.

In the second step, the rigidity constraint is applied to the solid region using the distributed Lagrange multiplier (DLM) technique to simulate the rigid body motion of solid particles [22]. The rigidity force is zero everywhere in the domain except in the particle domain where it is defined as

$$\mathbf{f}^m = \mathbf{f}_*^m + \mathbf{f}_c^m, \quad (4)$$

where $\mathbf{f}_c^m = -\alpha \rho_p (\mathbf{u} - \mathbf{w}_p^m) / \Delta t$ is the correction to the force from previous iteration, \mathbf{f}_*^m , α the relaxation parameter, Δt the time step, and $\mathbf{w}_p^m = \mathbf{W}_p^m + \boldsymbol{\omega}_p^m \times \mathbf{r}$ is the velocity in the m th particle. The translational velocity \mathbf{W}_p^m and the rotational velocity $\boldsymbol{\omega}_p^m$ of the particles are calculated as

$$M_p^m \mathbf{W}_p^m = \int \phi \rho_p^m \mathbf{u} dV, \quad (5)$$

$$\mathbf{I}_p^m \boldsymbol{\omega}_p^m = \int \phi \rho_p^m \mathbf{r} \times \mathbf{u} dV, \quad (6)$$

where M_p^m , \mathbf{I}_p^m , and ρ_p^m are the mass, moment of inertia, and density of the m th particle, respectively, and \mathbf{r} denotes the position vector measured from the center of the particle. The iteration on force is repeated until the normalized residuals fall below the specified tolerance of 10^{-3} .

Equations (1) to (3) are solved on a nonuniform staggered grid using the operator splitting technique. We found that at least 50 points in the diameter of the particle are needed to obtain grid-independent results for the vortex structures and near particle features of the flow. However, using 20 points across the diameter of the particles is enough to predict the global features of the motion such as velocity and displacement of the particles. The accuracy of the results are confirmed by convergence tests. In our simulations, domains of side lengths of $20d_p$ and $10d_p$ are used for side-by-side and in-line settling of particles in stratified fluids, respectively. We found that doubling the domain size results in less than 1% difference in the numerical results. Spatial discretization is implemented by quadratic upstream interpolation for convective kinetics (QUICK) scheme and the time increment is obtained using the

second-order Runge-Kutta method. In addition, the Courant-Fredrich-Levy (CFL) number of $O(0.1)$ is used to set the time step. The numerical method has been used and verified in our previous publications on the particle motion in viscous fluids [22–24].

A. Collision strategy

As two particles approach each other, high pressure is building up in the thin film between the particles. Improper capturing of this high pressure can lead to an unphysical situation in which particles overlap [25]. We implement a short-range repulsive force \mathbf{F}_R^m , as of Glowinski *et al.* [26], to avoid overlapping of the particles over the course of collision. Equation (5) is then modified as

$$\mathbf{W}_p^m = \frac{1}{M_p^m} \int \phi \rho_p^m \mathbf{u} dV + \frac{\mathbf{F}_R^m}{M_p^m} \Delta t, \quad (7)$$

where the repulsive force is defined as

$$\mathbf{F}_R^m = \frac{C_m}{\varepsilon} \left(\frac{R_m + R_n - |G_m G_n| + d_R}{d_R} \right)^2 \frac{\overrightarrow{G_m G_n}}{|G_m G_n|}, \quad (8)$$

where C_m is the characteristic force represented by $M_p^m g$; R_m and R_n are the radius of m th and n th particle, respectively; G_m and G_n are the position of the center of each particle; $|G_m G_n|$ is the distance between the particles; $d_R = h_\Omega$ is the force range; and $\varepsilon = h_\Omega^2$ is a small positive number where h_Ω denotes the smallest grid size in the computational domain [26]. The repulsive force is applied when the distance between the particles, i.e., $|G_m G_n| - R_m - R_n$, is smaller than d_R and is zero otherwise.

III. PARTICLE INTERACTION IN STRATIFIED FLUIDS

A. Side-by-side configuration

The side-by-side sedimentation of a pair of particles can be markedly affected by the properties of the fluid through which particles are settling. In a homogenous fluid, the separation distance of the settling particles increases due to the inertial effects whereas settling in viscoelastic fluids leads to the aggregation of the particles and chain formation [20]. Here, we characterize the role of density stratification on the settling dynamics of a pair of particles released from a side-by-side configuration. The particles are initially at rest and are separated by a prescribed distance S_0 in the transverse direction. Unless otherwise stated, the density ratio is $\rho_p/\rho_0 = 1.14$ where ρ_p denotes the density of the particle and ρ_0 is the background fluid density at the initial vertical position of particles (of the trailing particle in case of particles settling in tandem). Since the velocity of the particle is not known *a priori*, we scale dimensional velocity and time by the characteristic velocity and time that are defined as $W = \sqrt{gd_p}$ and $\tau = \sqrt{d_p/g}$, respectively. Based on this characteristic velocity, the Reynolds and Froude numbers are calculated as $Re = Wd_p/\nu$ and $Fr = W/Nd_p$, respectively. It is common practice in numerical literature investigating the settling motion of particles or drops or the rising motion of bubbles [25,27,28] to define the characteristic velocity as $\sqrt{gd_p}$. The undisturbed background density linearly changes with depth as $\rho_f(t=0) = \rho_0 - \gamma z$, where z is the vertical component of the position vector measured from the initial vertical position of particles (of the trailing particle in case

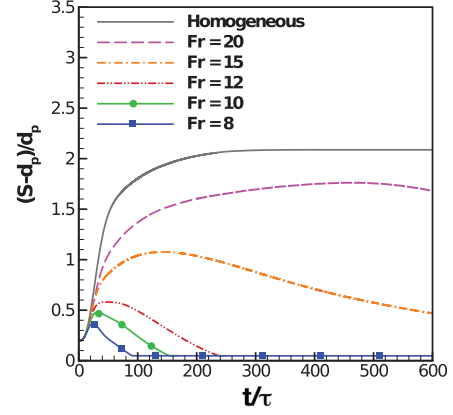


FIG. 1. (Color online) The temporal evolution of the distance between the particles as a function of the Froude number for $Re = 50$, $Pr = 700$, and $S_0 = 1.2d_p$.

of particles settling in tandem). The first comparison can be made by following the time evolution of the distance between the particles, S , for different Froude numbers (see Fig. 1). Initially, the distance between the particles increases due to the inertial effects analogous to the homogeneous fluid. Interestingly, however, the presence of the stratification hinders further repulsion between the particles and leads to their attraction. The buoyancy-induced attraction is followed by the particle collision after which particles descend together as a stable long body settling on its broad side. The attraction of the particles due to the stratification can be explained by analyzing the flow field around the settling particles. Figure 2 shows snapshots of contours of vorticity and the deformation of contours of constant density (isopycnals) for particles settling side-by-side in a linearly stratified fluid for $Re = 50$, $Fr = 10$, $Pr = 700$, and $S_0 = 1.5d_p$. The deflection of isopycnals behind the particles leads to the local nonalignment of the density gradients with the vertical direction $\hat{\mathbf{k}}$. This in turn results in the formation of secondary vortices and columnar structures behind each particle. The generation of the buoyancy-induced vortices is explained by the vorticity equation written under the Boussinesq approximation:

$$\frac{D\boldsymbol{\omega}}{Dt} = (\boldsymbol{\omega} \cdot \nabla) \mathbf{u} + \nu \nabla^2 \boldsymbol{\omega} - \frac{g}{\rho_0} \nabla \rho \times \hat{\mathbf{k}}, \quad (9)$$

where $\boldsymbol{\omega} = \nabla \times \mathbf{u}$ is the vorticity vector and the last term on the right-hand side represents the gravitational torque. As the particles settle down, the columnar structures behind the two particles collapse and form a rear vertical jet in the middle distance between the particles (see Supplemental Material movie 1 in Ref. [29]). The comparison of the velocity field of a homogeneous and a stratified fluid is shown in Fig. 3, representing distinct features of the flow signature in the presence of a background density gradient. The formation of the jet in the stratified fluid leads to the attraction between the particles. For smaller Froude numbers, the stronger attraction due to the strong stratified jet results in the collision of the particles earlier in time. Once the collision occurs, settling particles remain attached and decelerate due to the enhanced buoyancy force at higher density levels. The strength of the attraction between the particles depends upon the relative dominance of buoyancy and inertia along

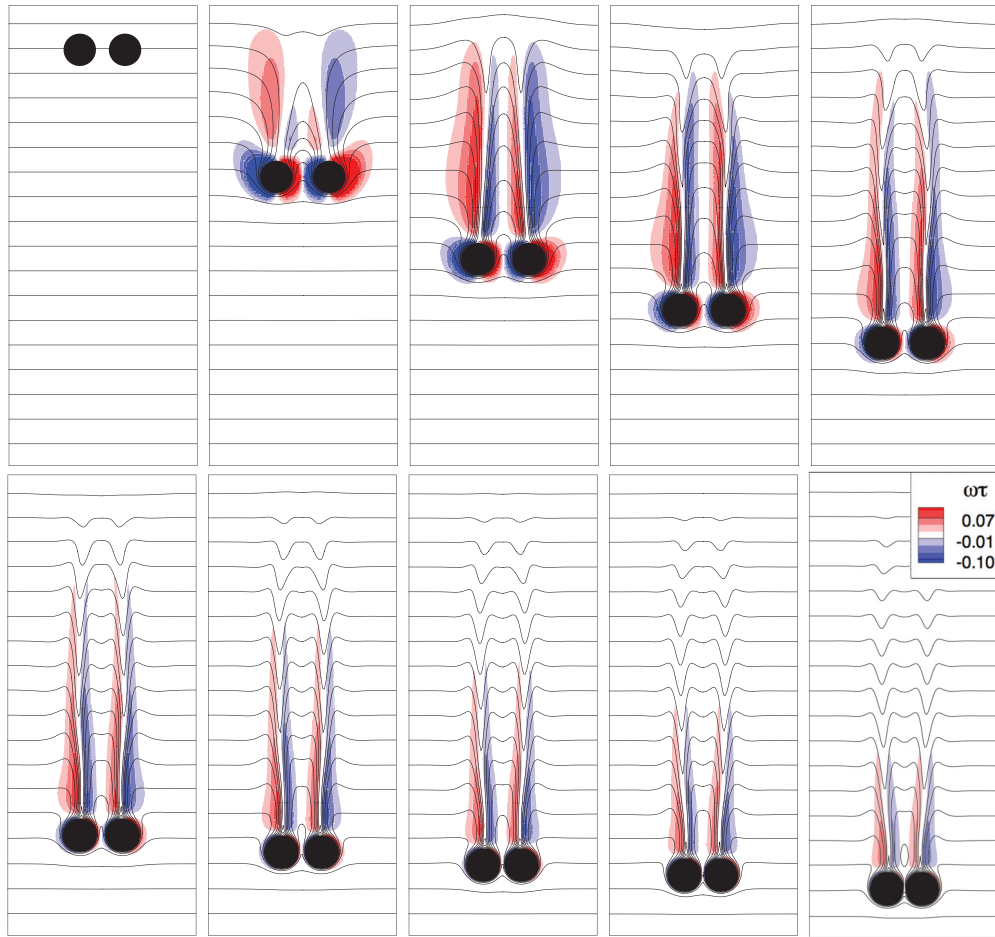


FIG. 2. (Color online) Snapshots of the particle motion for $Re = 50$, $Pr = 700$, $Fr = 10$, and $S_0 = 1.5d_p$. All frames are taken with dimensionless time increment of $\Delta t = 30$. The colormap shows contours of vorticity and black solid lines represent contours of constant density. The density difference between two adjacent black solid lines is $\Delta\rho/\gamma d_p = 1.2$.

with the strength of the diffusion in the stratified fluid. It is expected that the initial distance between the particles affect the interaction of the particle pair settling abreast. The effect of the initial distance is characterized in Fig. 4. As the initial offset between the particles is extended, the collision of the particles is postponed due to the delayed collapse of the rear

jets. The results indicate that, even for large values of the Froude number, the attraction between particles can occur and buoyancy effects eventually find their way in reducing the distance between the particles.

Furthermore, it is instructive to explore the role of the diffusivity of the stratifying agent on the side-by-side settling

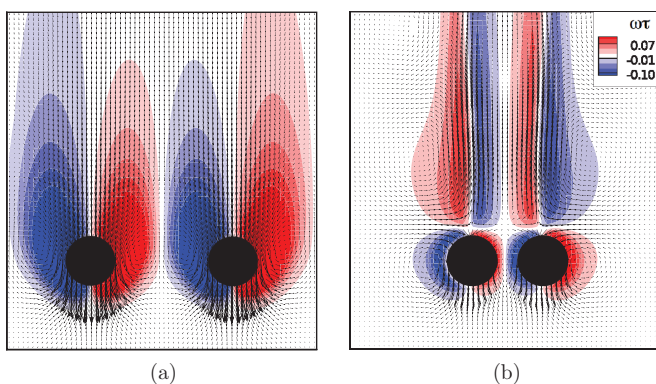


FIG. 3. (Color online) The detail of the velocity field and vorticity contours generated by settling of particles in a (a) homogeneous fluid and (b) stratified fluid. For both cases $Re = 50$, $S_0 = 1.5d_p$, $Pr = 700$, and $t/\tau = 115$. $Fr = 10$ for the stratified case.

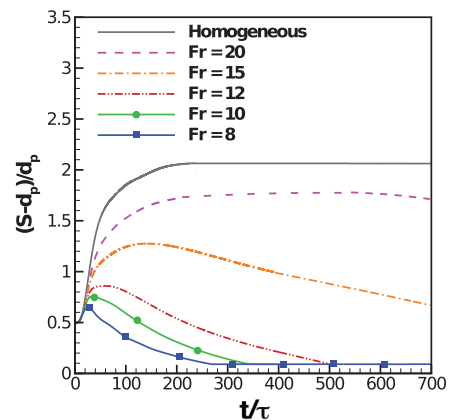


FIG. 4. (Color online) The temporal evolution of the distance between the particles settling side-by-side as a function of the Froude number for $Re = 50$, $Pr = 700$, and $S_0 = 1.5d_p$.

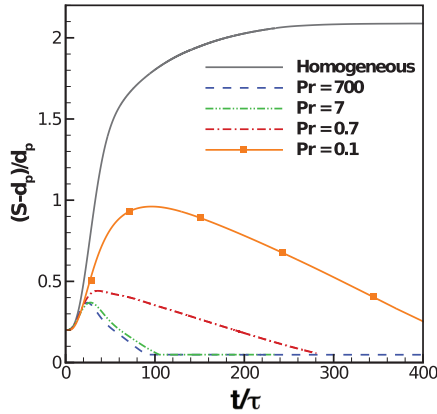


FIG. 5. (Color online) The temporal evolution of the distance between the particles as a function of the Prandtl number for $Re = 50$, $Fr = 10$, and $S_0 = 1.2d_p$.

of the particles. Figure 5 provides a comparison of the distance between the particles for $Re = 50$, $Fr = 10$, and $S_0 = 1.2d_p$ for different Prandtl numbers. The interaction of the particles is more sensitive to the diffusion of the stratifying agent at lower values of the Prandtl number. This can be rationalized by the strong diffusion effects at sufficiently small Prandtl numbers which strongly prohibit the accumulation of isopycnals in front of particles and weaken the buoyancy induced jet behind the particles.

In addition, we quantify the viscous effects by comparing transient behavior of the particles at a fixed Froude number for a range of Reynolds numbers (see Fig. 6). The particles are more rapidly separated as the Reynolds number increases. However, the particle separation is hindered at some distance where the stratification-induced attraction balances the inertial repulsion. As the Reynolds number increases, the inertial repulsion between the particles is stronger and it takes a longer time for the particles to touch. In summary, in stark contrast to a homogeneous fluid, particles settling side-by-side in linearly stratified fluids are attracted to each other as they sediment.

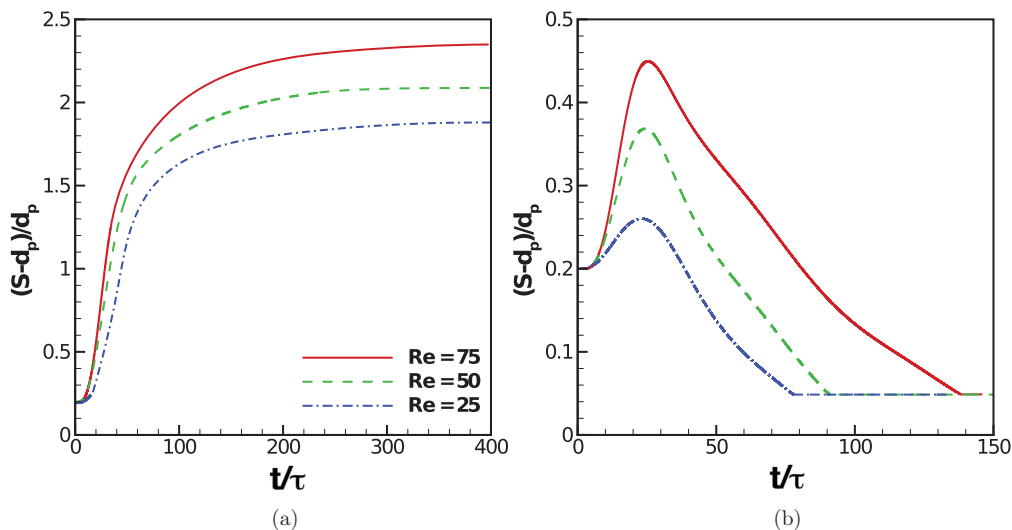


FIG. 6. (Color online) The role of Reynolds number on the time-dependent distance between the particles for $S_0 = 1.2d_p$ in (a) homogeneous fluid and (b) stratified fluid for $Fr = 10$ and $Pr = 700$.

B. Settling in tandem

Next we study the role of stratification on the in-line settling of the particles released from rest. The snapshots of the particle motion in a stratified fluid along with the deflection of isopycnals and contours of the vertical component of velocity are shown in Fig. 7 for $Re = 200$, $Fr = 12$, $Pr = 700$, and $S_0 = 2d_p$. As the particles accelerate from the initial position, the trailing particle is attracted into the wake of the leading particle. The drafting of the trailing particle continues until the particles touch similar to the drafting and kissing phases in a homogeneous fluid. In the next phase, however, instead of tumbling, the trailing particle bounces back and particles separate from each other, therefore drafting, kissing, and tumbling is replaced by drafting, kissing, and separation (see Supplemental Material movie 2 in Ref. [29]). The separation of particles after the kissing stage can be explained by the dynamics of the jet formation in a stratified fluid. Once the particles collide, the vertical velocity of the trailing particle drops. Meanwhile the restoration of the density layers behind the particle to their neutrally buoyant levels generates a columnar structure in the wake of the trailing particle. Subsequently, the upward buoyancy force due to the restoration of isopycnals dominates and the direction of the motion of the trailing particle is reversed for a short time. The reversal of motion for an isolated particle settling in stratified fluids has been previously reported in the literature [30]. Figure 8 shows the detailed velocity field and the structure of the jet at the time instance corresponding to the separation of particles after the collision. Figure 9(a) shows that particles collide again at time $t/\tau = 300$ and settle together till they reach their neutrally buoyant level.

Figures 9(a) and 9(b) show the temporal variation of the vertical velocity of the particles along with the corresponding distance between the particles as a function of the Froude number. As the Froude number decreases, the kissing stage does not occur and the interaction is characterized by drafting followed by the particle separation. This is attributed to the stronger buoyancy forces leading to the generation of buoyancy-induced columnar structures and the reversal of the

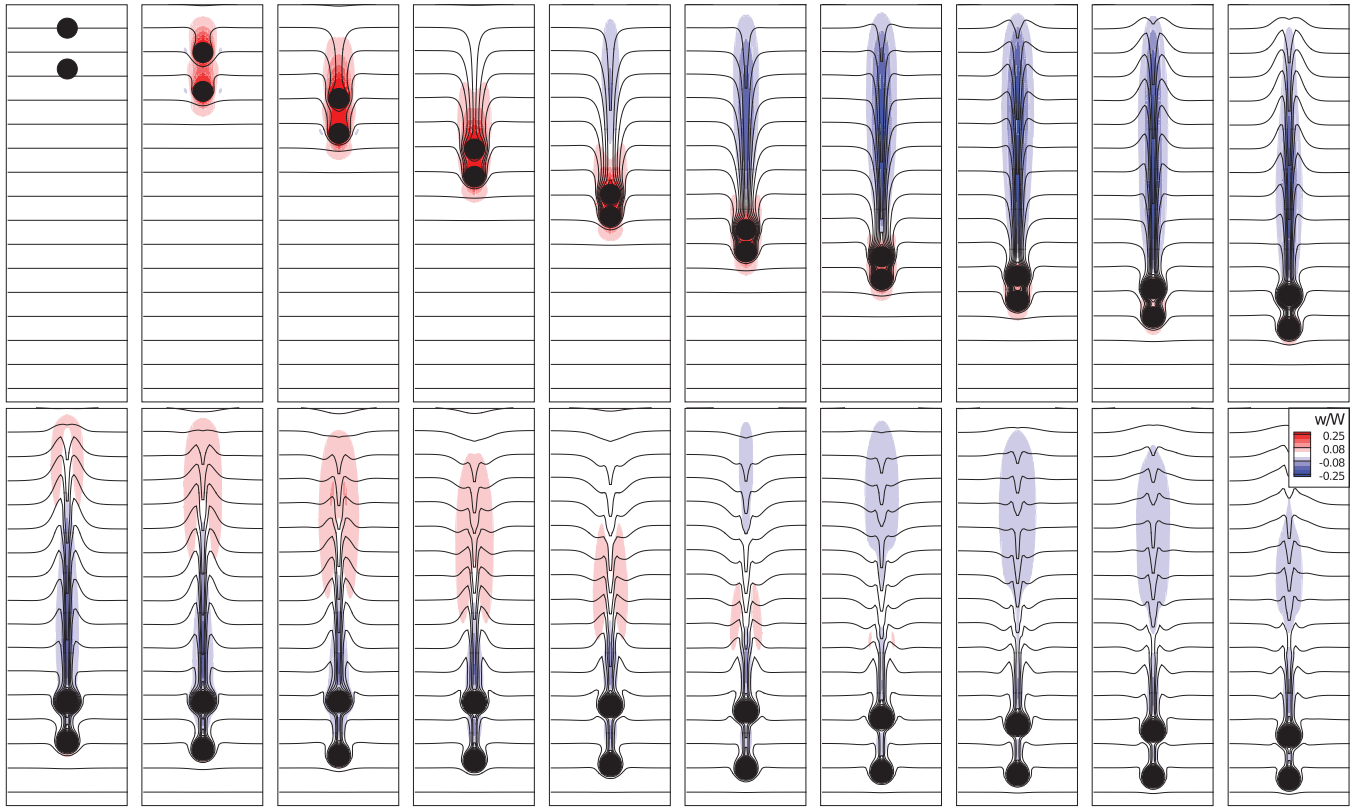


FIG. 7. (Color online) Snapshots of the in-line motion of particles for $Re = 200$, $Pr = 700$, $Fr = 12$, and $S_0 = 2d_p$. All frames are taken with dimensionless time increment of $\Delta t = 7.7$. The colormap shows contours of vertical component of velocity and black solid lines represent contours of constant density. The density difference between two adjacent black solid lines is $\Delta\rho/\gamma d_p = 1.2$

motion of the trailing particle before particles touch (kissing stage). The separation of the particles initiates earlier in the presence of a strong background density gradient, however, the maximum distance between the particles reduces due

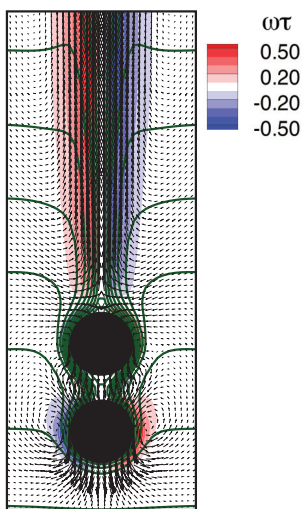


FIG. 8. (Color online) The closeup of the structure of the buoyancy induced jets at time $t/\tau = 61.6$ for $Fr = 12$, $Re = 200$, $Pr = 700$, and $S_0 = 2d_p$. The velocity vectors, vorticity contours (colormap), and contours of constant density (green solid lines) are shown. The density difference between two adjacent green solid lines is $\Delta\rho/\gamma d_p = 1.2$

to smaller velocities of the particles. This emphasizes the importance of the mutual impact of inertia and buoyancy on classifying the type of interaction in stratified fluids. The particle pair interaction can be further characterized by plotting particle velocity versus the dimensionless density ratio [see Fig. 9(c)]. The dimensionless density ratio is defined as $1 - (\rho_p - \rho_b)/(\rho_p - \rho_0)$, where it is unity at the neutrally buoyant position of the trailing particle and zero at its initial position. Here, ρ_b is the undisturbed background density at the instantaneous location of the trailing particle [$\rho_f(t = 0)$ at the location of the trailing particle is ρ_b]. The reversal of the particle motion, also referred to as levitation, is easily distinguished in this plot as a loop. The lower the Froude number, the levitation initiates at lower density levels and the generation of the jet is expedited. As the Reynolds number decreases, the viscous dissipation more effectively suppresses the inertial effects and the separation of particles initiates even before the kissing stage occurs (Fig. 10). Moreover, after the separation phase takes place, the repulsion between particles becomes weaker as the Reynolds number decreases.

For relatively larger values of the Froude number, the inertia dominates the buoyancy effects and drafting, kissing, and tumbling governs the particle interaction [see Fig. 11(a)]. The transition between drafting-kissing-tumbling and drafting-kissing-separation occurs at $Fr \approx 12$. Even though for a weak stratification a qualitatively similar interaction dynamics as in the homogeneous fluid is recovered, the postcollision dynamics is affected by the stratification and a

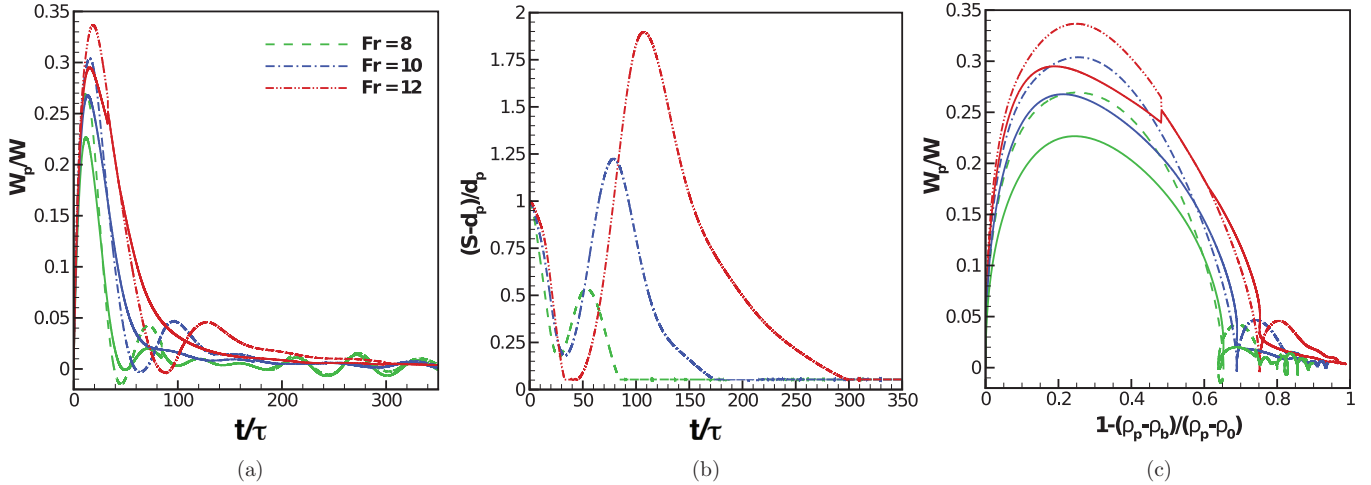


FIG. 9. (Color online) The interaction dynamics of a pair of particles settling in tandem as a function of the Froude number for $Re = 200$, $Pr = 700$, and $S_0 = 2d_p$; (a) the temporal evolution of the settling velocity; (b) the transient variation of the distance between the particles; (c) the variation of the velocity as a function of the dimensionless background density at the instantaneous position of the particles. Solid lines and dashed lines represent the velocity of the leading and trailing particles, respectively.

prolonged kissing time is observed. Thus, following the initial attraction and subsequent collision, particles remain attached for a longer period of time in a stratified fluid compared to the homogeneous counterpart. This prolonged kissing stage can be associated with the reduction of the instantaneous Reynolds number of the particles in a stratified fluid. In the limit of vanishingly small Reynolds number, the orientation and distance of settling particles remain constant. We quantify the prolonged kissing time by measuring the distance and the temporal evolution of the angle between the particles line of centers and the vertical line [see Figs. 11(b) and 11(c)]. The stronger stratification more effectively reduces the rotation rate of the elongated configuration. The prolonged kissing time can have important consequences on the sedimentary fluxes and the aggregation rates of particles in industrial and environmental fluids that are characterized by density stratification.

The results show the role of stratification on the interaction of a pair of particles. This can have an important consequence

on the microstructure of the suspensions of particles in stratified fluids. A measure of microstructure can be obtained by the pair correlation function which shows the excess of close pairs at large times for the suspension of spherical particles settling in homogeneous fluids at the Stokes' regime [31]. We expect the excess of close pairs to be even larger in stratified fluids compared to homogenous fluids. The present work can be extended to reveal the role of stratification on the pair correlation function of the suspension of spheres sedimenting in a stratified fluid and it will be the focus of our future works. Also it is noteworthy to mention that Caffisch and Luke [32] studied dilute suspensions of sedimenting spheres under Stokes conditions and showed that the variance in settling speed diverges with the size of the container. Gómez *et al.* [33] showed that the stratification in the particle concentration suppresses velocity fluctuations under certain conditions. Even though the topic of this paper is different and focuses on the role of density stratification of the background fluid on the interaction of settling particles (rather than the stratification in the concentration of the particles), we expect that the density stratification of the background fluid also suppresses velocity fluctuations in a suspension of spheres sedimenting in a density stratified fluid.

IV. CONCLUSION

The comprehensive understanding of the fluid mechanics of environmental and geophysical phenomena requires the detailed information on particle-particle and particle-fluid interactions in stratified fluids. Here, we have shown that the presence of the vertical density gradients in fluids can substantially alter the characteristics of the particle pair interaction. We have characterized the role of stratification in the settling of the particles in two general configurations. We have demonstrated that for the side-by-side sedimentation of the particles, the stratification induces the attraction between the particles and even for large values of Froude numbers

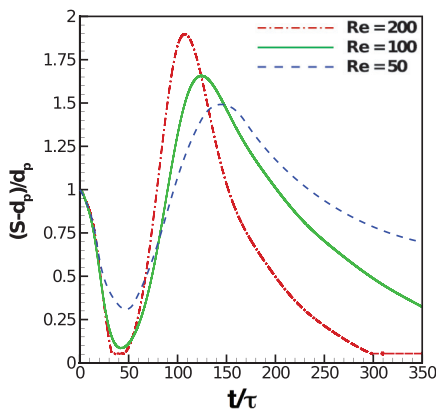


FIG. 10. (Color online) The role of Reynolds number on the time-dependent distance between the particles settling in tandem for $Fr = 12$, $Pr = 700$, and $S_0 = 2d_p$.

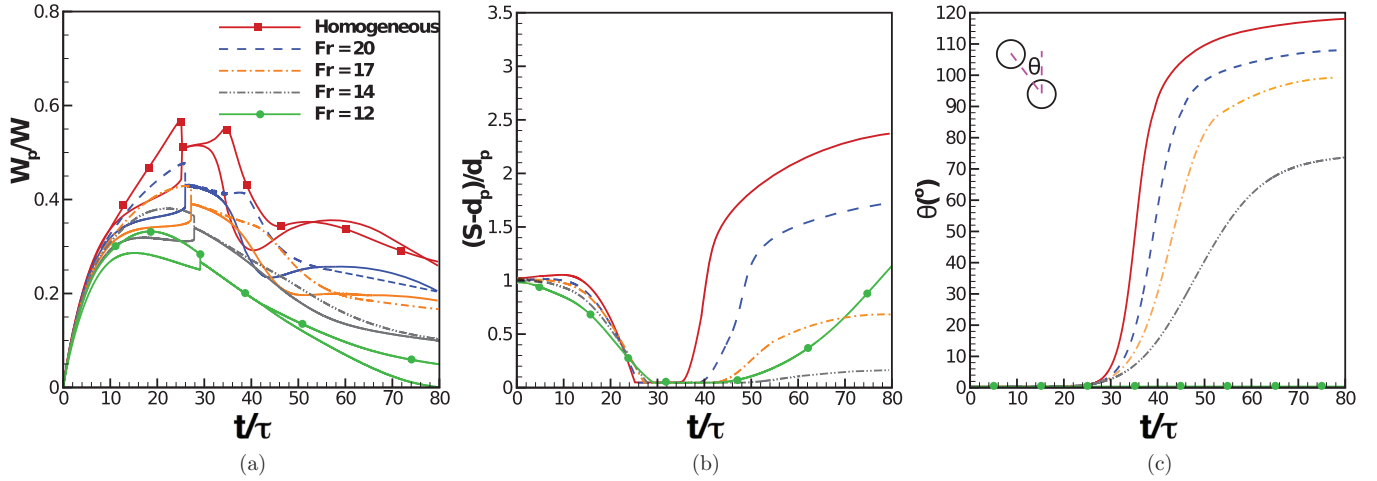


FIG. 11. (Color online) The temporal evolution of (a) the vertical velocity of the particles, (b) the distance between the particles, and (c) the orientation of the particles are plotted for $Re = 200$, $Pr = 700$, and $S_0 = 2d_p$. Solid lines and dashed lines represent the velocity of the leading and trailing particles, respectively.

the distance between the settling particles is reduced by buoyancy effects over a long period of time. The attraction of the particles has been explained by the interaction of the buoyancy-induced jets behind the particles and corresponding jet formation in between the particles. We have quantified the importance of the key physical mechanisms by characterizing the interaction for a wide range of Reynolds, Prandtl, and Froude numbers. In addition, we have presented the role of buoyancy effects on the interaction dynamics for the particles settling in tandem. We documented that drafting, kissing, and tumbling is replaced with drafting, kissing, and separation due to the formation of columnar structures in the stratified fluids. Moreover, we have illustrated the decisive role of stratification in eliminating the kissing stage at small values of Froude numbers. We have shown that for the cases of weak stratification in which drafting, kissing, and tumbling occurs, the postcollision dynamics can be strongly affected by stratification and a prolonged kissing time is observed. The importance of the results presented here can be highlighted by considering the sedimentation of particles in natural environments. Experimental measurements of sedimentary fluxes of marine snow particles have reported marine snow ranging in size from 0.5 to 75 mm, settling at rates ranging from 16 to 386 m/day [4,34,35]. This corresponds to Reynolds numbers ranging from 0.1 to 335 and Froude numbers ranging from 0.2 to 812 in a moderate stratification ($N = 0.011 \text{ s}^{-1}$). Thus, for instance, the interaction of particles of the size 30 mm, sinking at 200 m/day, ($Re = 69, Fr = 7$), will be significantly affected by the effects of stratification.

The attraction of particles settling side-by-side, longer kissing time, and enhanced number of collisions for particles settling in tandem demonstrate new mechanisms of accumulation of particles and aggregation of organisms at local hot spots in aquatic environments characterized by density stratification. Particle aggregation initiated by the hydrodynamic interaction of particles in stratified fluids can be further enhanced by short-range attraction forces (e.g., van der Waals, electrostatics) and can lead to the formation and persistence of marine snow

layers leading to accumulation of swimming plankton [6] and formation of thin phytoplankton layers.

ACKNOWLEDGMENT

This work is supported by NSF Grant No. CBET-1066545.

APPENDIX: VERIFICATION AND VALIDATION OF THE NUMERICAL METHOD

1. Settling of a spherical particle in a homogeneous fluid

We first compare the results of the numerical scheme with experimental measurements of the settling velocity of spherical particles by Mordant and Pinton [36]. The physical parameters are set in such a way as to ensure that the density ratio $\rho_p/\rho_0 = 2.56$ and the Reynolds number $Re = 39.35$ match the experiments. The characteristic velocity $W = \sqrt{gd_p}$ is used to define the Reynolds number. A computational domain of size $8d_p \times 8d_p \times 64d_p$ is used with a grid resolution of 12 points across the particle diameter. The comparison

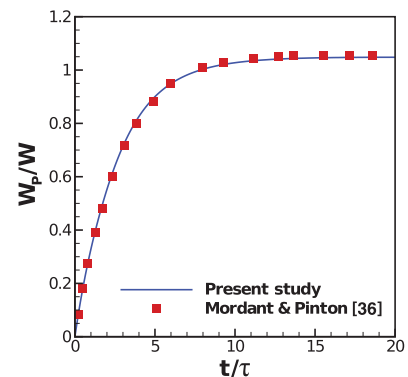


FIG. 12. (Color online) The transient variation of the settling velocity of a sphere in a homogeneous fluid.

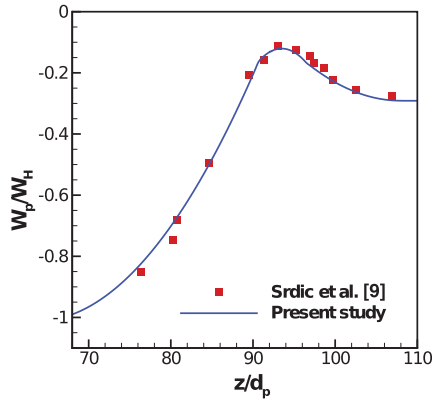


FIG. 13. (Color online) Settling velocity of a spherical particle as a function of distance fallen in a sharply stratified fluid.

of the settling velocity of the particle as a function of time for experimental and numerical studies shows a very good agreement (see Fig. 12).

2. Settling of a sphere through sharp density interfaces

Next we validate the numerical scheme against the experimental study of Srđić, Mohamed, and Fernando [9] on the sedimentation of particles through density interfaces. The density ratio, $\rho_p/\rho_0 = 1.048$, the Reynolds number, $Re = 127$, the Prandtl number, $Pr = 740$, and the buoyancy jump, $\Delta\rho/\rho = 6.47 \times 10^{-2}$ are set equivalent to the values of the experiment. The Reynolds number is defined based on $W = \sqrt{gd_p}$ as a characteristic velocity. A large computational domain of size $10d_p \times 10d_p \times 160d_p$ is implemented with a grid resolution of 20 points across the diameter of the particle. The results of the numerical scheme for the spatial variation of the settling velocity closely matches the results of Srđić, Mohamed, and Fernando (see Fig. 13). After reaching

the terminal velocity in the upper layer fluid, the particle decelerates at the interface to a minimum velocity and then accelerates toward the terminal velocity in the lower, heavier fluid.

3. Drafting-kissing-tumbling in a homogeneous fluid

Finally, we compare the time-dependent settling velocity of the particles with the numerical simulations of Glowinski *et al.* [26] for two identical spheres sedimenting in an incompressible Newtonian fluid. The computational domain of the size $\Omega = [0, 1] \times [0, 1] \times [0, 4]$ cm³ is used. The particles are initially located at $\mathbf{X}_p^1(t = 0) = (0.5, 0.5, 3.16)$ cm and $\mathbf{X}_p^2(t = 0) = (0.5, 0.5, 3.50)$ cm, where \mathbf{X}_p^1 and \mathbf{X}_p^2 denote the location of the particles. The ratio of the density of the particles to the fluid density is $\rho_p/\rho_f = 1.14$ and the particles have the same diameter, $d_p = 1/6$ cm. The particles are initially at rest and fall due to the gravitational acceleration, $\mathbf{g} = (0, 0, -981)$ cm/s², in a fluid with kinematic viscosity of $\nu = 0.01$ cm²/s. The Reynolds number based on $W = \sqrt{d_p g}$ is $Re = 213$. The grid size of $h_\Omega = 1/80$ cm is used and the time step is adjusted during the run time using $CFL = 0.25$, giving a typical value of $\Delta t = O(10^{-4})$ s during the simulation.

Figure 14 represents the variation in the vertical velocity, the distance, and the orientation of the particles as a function of the settling time. The results are presented in dimensionless form using $W = \sqrt{d_p g}$ and $\tau = \sqrt{d_p/g}$ as the characteristic velocity and the characteristic time, respectively. The results are in excellent agreement with the previous numerical results up to the point that collision takes place. The difference in the postcollision vertical velocity of different numerical methods is not unexpected because of the strong instability of the tumbling stage which leads to a distinct quantitative kissing time for different numerical simulation and is a well known effect in the numerical simulation of the drafting, kissing, and tumbling phenomenon [25,37].

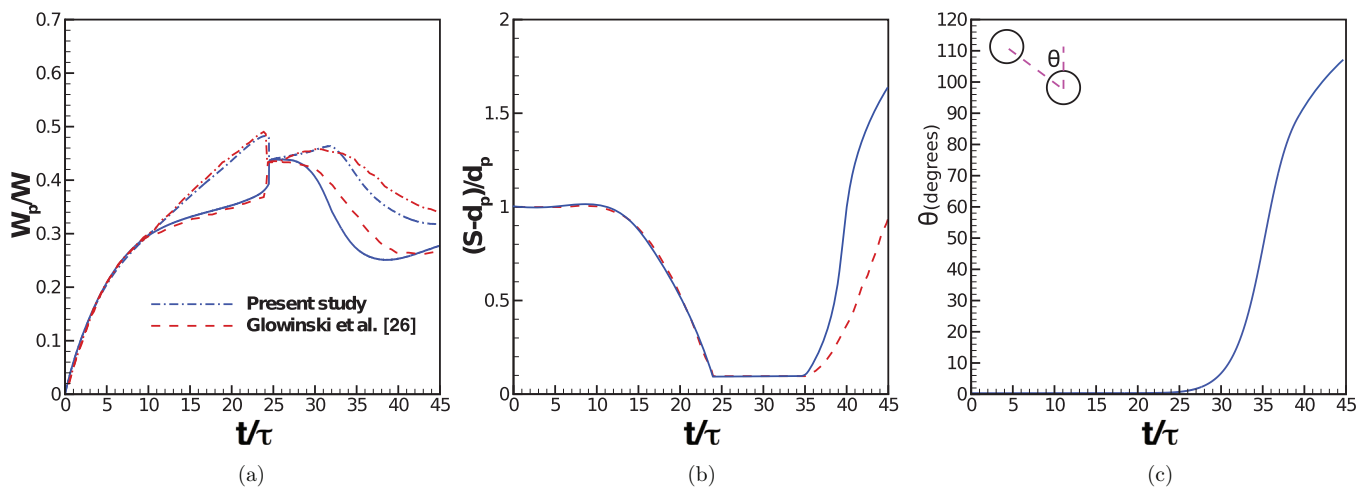


FIG. 14. (Color online) The transient variation of (a) the vertical velocity of the particles, (b) the distance between the particles, and (c) the orientation of the particles as they undergo drafting, kissing, and tumbling. In (a), dash-dot lines represent the velocity of the trailing particle.

- [1] W. W. Kellogg, *Aerosols and Climate*, edited by W. Bach *et al.* (Kluwer, Dordrecht, The Netherlands, 1980), Chap. In Interactions of Energy and Climate, pp. 281–296.
- [2] A. P. Lisitzin, *Oceanic Sedimentation: Lithology and Geochemistry* (AGU, Washington, DC, 1996).
- [3] H. J. S. Fernando, M. S. Lee, J. Anderson, M. Princevac, E. Pardyjak, and S. Grossman-Clarke, *Env. Fluid Mech.* **1**, 107 (2001).
- [4] J. T. Turner, *Aquat. Microb. Ecol.* **27**, 57 (2002).
- [5] S. C. Lefebvre, I. Benner, J. H. Stillman, A. E. Parker, M. K. Drake, P. E. Rossignol, K. M. Okimura, T. Komada, and E. J. Carpenter, *Glob. Change. Biol.* **18**, 493 (2011).
- [6] A. L. Alldredge and C. C. Gotschalk, *Deep-Sea Res. Part A* **36**, 159 (1989).
- [7] R. Lindsey and M. Scott, NASA Earth Observatory Project (2010), <http://earthobservatory.nasa.gov/Features/Phytoplankton>.
- [8] A. Doostmohammadi, R. Stocker, and A. M. Ardekani, *Proc. Nat. Acad. Sci.* **109**, 3856 (2012).
- [9] A. N. Srdić-Mitrović, N. A. Mohamed, and H. J. S. Fernando, *J. Fluid Mech.* **381**, 175 (1999).
- [10] R. Camassa, C. Falcon, J. Lin, R. M. McLaughlin, and R. Parker, *Phys. Fluids* **21**, 031702 (2009).
- [11] R. Camassa, C. Falcon, J. Lin, R. M. McLaughlin, and N. Mykins, *J. Fluid Mech.* **664**, 436 (2010).
- [12] C. R. Torres, H. Hanazaki, J. Ochoa, J. Castillo, and M. Van Woert, *J. Fluid Mech.* **417**, 211 (2000).
- [13] H. Hanazaki, K. Konishi, and T. Okamura, *Phys. Fluids* **21**, 026602 (2009).
- [14] K. Y. Yick, C. R. Torres, T. Peacock, and R. Stocker, *J. Fluid Mech.* **632**, 49 (2009).
- [15] A. M. Ardekani and R. Stocker, *Phys. Rev. Lett.* **105**, 084502 (2010).
- [16] H. Hanazaki, K. Kashimoto, and T. Okamura, *J. Fluid Mech.* **638**, 173 (2009).
- [17] J. W. M. Bush, B. A. Thurber, and F. Blanchette, *J. Fluid Mech.* **489**, 29 (2003).
- [18] A. F. Fortes, D. D. Joseph, and T. S. Lundgren, *J. Fluid Mech.* **177**, 467 (2006).
- [19] M. J. Riddle, C. Navarez, and R. B. Brid, *J. Non-Newtonian Fluid Mech.* **2**, 23 (1977).
- [20] D. D. Joseph, Y. J. Liu, M. Poletto, and J. Feng, *J. Non-Newtonian Fluid Mech.* **54**, 45 (1994).
- [21] A. M. Ardekani, R. H. Rangel, and D. D. Joseph, *Phys. Fluids* **20**, 063101 (2008).
- [22] A. M. Ardekani, S. Dabiri, and R. H. Rangel, *J. Comput. Phys.* **227**, 10094 (2008).
- [23] A. M. Ardekani and R. H. Rangel, *J. Fluid Mech.* **596**, 437 (2008).
- [24] A. M. Ardekani, S. Dabiri, and R. H. Rangel, *Phys. Fluids* **21**, 093302 (2009).
- [25] M. Uhlmann, *J. Comput. Phys.* **209**, 448 (2005).
- [26] R. Glowinski, T. W. Pan, T. I. Hesla, D. D. Joseph, and J. Periaux, *J. Comput. Phys.* **169**, 363 (2001).
- [27] B. Bunner and G. Tryggvason, *J. Fluid Mech.* **466**, 17 (2002).
- [28] V. Roig, M. Roudet, F. Risso, and A.-M. Billet, *J. Fluid Mech.* **707**, 444 (2012).
- [29] See Supplemental Material at <http://link.aps.org/supplemental/10.1103/PhysRevE.88.023029> for movies.
- [30] N. Abaid, D. Adalsteinsson, A. Agyapong, and R. M. McLaughlin, *Phys. Fluids* **16**, 1567 (2004).
- [31] B. Cichocki and K. Sadlej, *J. Stat. Phys.* **132**, 129 (2008).
- [32] R. E. Caflisch and J. H. Luke, *Phys. Fluids* **28**, 759 (1985).
- [33] D. C. Gómez, L. Bergougnoux, É. Guazzelli, and J. Hinch, *Phys. Fluids* **21**, 093304 (2009).
- [34] A. L. Alldredge and C. C. Gotschalk, *Limnol. Oceanogr.* **33**, 339 (1988).
- [35] J. R. Kilps, B. E. Logan, and A. L. Alldredge, *Deep-Sea Res. Part A* **41**, 1159 (1994).
- [36] N. Mordant and J. F. Pinton, *Eur. Phys. J. B* **18**, 343 (2000).
- [37] N. Sharma and N. A. Patankar, *J. Comput. Phys.* **205**, 439 (2005).